CHAPTER 3

Radiative transfer modeling in the cryosphere

Roberto Furfaro, Alberto Previti, Paolo Picca, Jeffrey S. Kargel, and Michael P. Bishop

ABSTRACT

Radiative transfer (RT) modeling plays a key role in interpreting the radiance measured by multispectral sensors. Glaciers respond to variations in solar irradiance. At-sensor radiance depends upon glacier surface material composition and intermixture of materials, solar and sensor geometry, and surface topography. To bridge the gap between investigative findings and spectral data, a physically based (i.e., based on first principles) linkage between properties of the observed surface and the measured electromagnetic signal should be established. Complementing the treatment of related subjects in Chapter 2 of this book by Bishop et al., in this chapter we show how RT theory can be adapted to derive radiative transfer equations (RTEs) that are commonly employed to properly describe the radiative field within, at the surface of, and above glaciers, debris fields, and glacier lakes. RTEs are derived using the basic principle of conservation of photons and are simplified to obtain equations that are more mathematically tractable. Such equations are numerically solved to compute quantities that are of interest in remote sensing (e.g., bidirectional reflectance factor, BRF, and spectral albedo) that are a function of the optical properties of the observed surface. Accurate modeling of the optical properties of single-material particles (e.g., ice or snow, water, lithic debris, and carbon soot) is critical to obtaining meaningful and accurate RT calculations. The common methods employed to determine single-scattering albedo and scattering phase function, for both single-type particles and mixtures, are discussed. In addition, although the basic conservation of photons holds for both glaciers and glacier lake water, we have marked a clear distinction between the equation of transfer for glacier surfaces and glacier lake water, as well as between the methods employed to describe their optical properties. The chapter also provides examples of RT-based calculations for both BRF and spectral albedo in scenarios typically found in the cryosphere. Five simulation sets show how remotely measurable quantities depend on the morphological and mineralogical properties of the medium (e.g., BRF for mixtures of snow and debris; spectral albedo variation for snow and carbon soot with varying grain size and particle concentration; and spectral variation of glacier lake water reflectance as a function of rock "flour" concentration).

3.1 INTRODUCTION

Remote sensing of the Earth's cryosphere is an active research area, as glaciological processes are closely linked to atmospheric, hydrospheric, and lithospheric processes (Bush 2000, Shroder and Bishop 2000, Meier and Wahr 2002) and a host

J. S. Kargel et al. (eds.), *Global Land Ice Measurements from Space*, Springer Praxis Books,
DOI: 10.1007/978-3-540-79818-7_3,

of issues of practical human concern. Global understanding of cryospheric processes involves analysis of glacier dynamics since they are affected by and can influence climate change (Kotlyakov et al. 1991, Seltzer 1993, Haeberli and Beniston 1998, Maisch 2000). Thus, characterization and estimation of glacier surface properties, such as ice grain size, rock debris cover, and surface water distribution, become critical to advancing our understanding of glacier–climate relationships and glacier fluctuations (Bishop et al. 2004, Kargel et al. 2005).

Because of the ability of orbiting platforms to provide global and continuous coverage of vast portions of Earth's surface, satellite imagery can be processed to extract information about important surface properties. Most space-based sensors operate passively, measuring the magnitude of reflected/emitted surface radiance in the visible, infrared, and thermal portions of the spectrum. The Advanced Spaceborne Thermal Emission and reflection Radiometer (ASTER), Moderate Resolution Imaging Spectrometer (MODIS), Polarization and Directionality of Earth Reflectance instrument (POLDER), and Multi-angle Imaging SpectroRadiometer (MISR) are examples of current space-based instruments that collect such multispectral data. Each of these instruments can record the directionality and intensity of surface radiance, thereby recording information about scattering properties that are a function of wavelength. For icy surfaces on Earth, we require spatial and temporal information about: (1) the amount of clear and dirty ice; (2) snow coverage and rock debris (including both patchy and intimate mixtures); (3) the distribution of ponded or flowing water; (4) the liquid water content of snow and grain size of snow and ice; and (5) the extent of partial vegetation cover (Kargel et al. 2005). These compositional and phase-state parameters are critical to characterizing the current state and recent dynamics of glaciers and, consequently, they are key to obtaining a better understanding of the processes associated with the cryospheric impacts of climate change.

Quantitative characterization of surface properties using remotely sensed data requires the definition of a functional relationship between surface properties and surface radiance. The bidirectional reflectance distribution function (BRDF) and/or the closely related bidirectional reflectance factor (BRF), as well as the spectral albedo, are the typical parameters employed to describe surface reflectance given irradiance, surface morphology, and composition variations. Glacier surfaces are generally comprised of a variety of materials and exhibit a complex reflectance distribution depending upon the spatial structure of surface constituents. Spatial and temporal variations in debris cover and intimate or areal mixtures between coarse-grained glacier ice, snow, liquid water, vegetation, and rock debris contribute to highly variable reflectance as observed by in situ and platform-based sensors (Kargel et al. 2005). Modeling plays a central role in investigating the relationships between surface mixtures and reflectance, and can assist glacier mapping and characterization. BRDF and BRF modeling are important functional components of scientific inquiry because they help bridge the gap between investigative findings and field-based and remote observations. For example, Mishchenko et al. (1999) modeled the directional reflectance pattern and its effect on albedo for four types of soils, each characterized by a different index of refraction. The BRF patterns were generated for snow using three different scattering phase functions (hexagonal ice, fractal ice, and spherical ice) to examine the effect of ice morphology on reflected radiation.

Models can also be used to provide a basis for surface parameter retrieval. For example, Piatek et al. (2004) use model inversion and laboratory-based data to extract the basic optical properties of regolith as a function of the chemical composition and grain size. Radiative transfer modeling was also used by Painter et al. (2003) to generate a lookup table comprising BRF patterns for spherical ice with variable grain size. Each of the elements of the lookup table was considered an endmember of the ice family, and a linear unmixing algorithm was used to map grain-size distribution over alpine glaciers.

Radiative transfer (RT) theory is the logical quantitative framework and physical basis for modeling spectral and directional reflectance as a function of surface composition and granular texture. Its theoretical basis was established by the seminal work of Chandrasekhar (1960), who derived the basic radiative transfer equation (RTE) describing the transport of photons moving in a generic medium characterized by specified optical properties. He also derived a set of techniques to determine analytical and numerical solutions for a large variety of radiative transfer problems. Whereas the RTE is capable of describing the radiative regime within a prescribed host medium, most of the efforts involving solutions of the RTE focused

on determining the number of photons reflected by a planetary surface as a function of incident radiation, viewing geometry, and surface properties. The goal was to provide a means for quantitative interpretation of the signal collected by airborne and/or spaceborne instruments. For example, Hapke (1981, 1986, 1993, 2002, 2008) devised a semi-empirical RTE-based bidirectional reflectance model that, under simplifying assumptions, allowed the analytical computation of the surface reflectance factor and other photometric properties of interest. The Hapke model has been successful in modeling the reflectance factor of a variety of planetary surfaces in the solar system (e.g., Helfenstein et al. 1988, Warell et al. 2009) and it is very popular in the planetary science community.

More recently, Mishchenko et al. (1999) devised an efficient and accurate BRF model that computes surface reflectance without the need to evaluate the light field within the particulate surface. Accurate numerical models that solve the RTE to determine both the light field within and reflected by the surface under investigation are also available. The most popular model is DISORT (Stamnes et al. 1988), which is a generic RT code capable of simulating the transport of photons in layered media with specified composition and optical thickness. A new multi-layer RT model based on recent theoretical and numerical advancements in solving the RTE (Siewert 2000) has been developed and tested against currently available codes (Previti 2010; Previti et al. 2011; Picca et al. 2007, 2008a, Picca 2009). Whereas the new model is general enough to model atmospheric RT, the Multi-layer Analytic Discrete Ordinate Code (MADOC; Furfaro et al. 2014) has been originally conceived to specifically model the radiation regime within glacier environments.

This chapter focuses on a fundamental treatment of RT principles and the modeling of the radiation reflected by glacier surfaces over the spectral range between 0.4 and 2.5 μm (VIS/NIR). We emphasize the processes required to compute surface reflectance (e.g., BRF and BRDF) and spectral albedo, which are the most meaningful parameters in optical remote sensing of Earth and planetary surfaces. In Section 3.2, the principles of RT are introduced and explained with special emphasis on a modeling approach to adapt the generic RTE to properly describe the radiative regime for glacier surfaces and glacier lakes. In Section 3.3, we provide a thorough description of the optical properties of materials comprising a glacier surface (snow, ice, rock debris) and, separately, the optical properties of glacier water. Methods currently employed to model the optical properties of mixtures are also reported. Section 3.4 briefly reviews the variety of numerical methods available to solve the RTE and discusses some of the RT codes available in the literature. We then show some examples of simulations of albedo and BRF for a variety of scenarios that are typically found on glacier surfaces.

3.2 RADIATIVE TRANSFER MODELING OF GLACIER SURFACES

Modeling the radiative regime of glacier surfaces requires a quantitative understanding of how photons interact with complex surface compositions. RT theory provides the physical basis for modeling spectral and directional reflectance as a function of composition and granular texture. The RT problem and its mathematical machinery were initially developed by Chandrasekhar (1960), who applied the model to the transfer of light in atmospheres, oceans, and the interstellar medium. Here, we are interested in detailing a modeling approach that yields RT equations capable of quantifying the light reflected and transmitted by glaciers and glacier lakes.

We begin by considering the general problem. Sunlight is comprised of photons traveling through the atmosphere. Ultimately, they reach the Earth's surface and interact with media such as that of the surface of a glacier. The host medium is usually characterized by an ensemble of particles with properties that are a function of their composition and spatial arrangement. Commonly, such ensembles of particles include ice ranging from multicentimeter glacier ice to fine-grained snow and frost, liquid water, suspended particles in the water, and rock debris or soot resting on the glacier or intermixed in the optical zone of the ice and snow. The ensembles are modeled here as dense particulate media that are illuminated by both direct and diffuse beams of photons and whose optical properties can be individually described by a finite number of parameters. Such parameters are intended to describe how the medium interacts with light particles. Generally, photons are either absorbed or scattered. A single photon can undergo multiple scattering before it is either absorbed by, or exits from the medium back into the atmosphere and space. Modeling radiative

transport in dense particulate media is commonly done either stochastically or deterministically. Here, we will utilize a deterministic modeling approach that consists in formulating an integro-differential equation derived from a fundamental law of physics (i.e., the balance of photons in the appropriate phase space). In classical RT theory, the medium is assumed to be a collection of dimensionless scattering and absorbing centers uniformly distributed in a differential volume. The photons' behavior is determined by the probability of scattering and/or absorption within the host medium, assuming that streaming is possible between interactions. If the conservation of photons is applied in six-dimensional phase space (i.e., position and velocity), the following equation is utilized:

$$\frac{1}{c}\frac{\partial I_\lambda(\boldsymbol{r},\boldsymbol{\Omega},t)}{\partial t}+\boldsymbol{\Omega}\cdot\nabla I_\lambda(\boldsymbol{r},\boldsymbol{\Omega},t)+\Sigma_{tot}(\boldsymbol{r})I_\lambda(\boldsymbol{r},\boldsymbol{\Omega},t) = \frac{1}{4\pi}\int d\boldsymbol{\Omega}'\,\Sigma_s(\boldsymbol{r},\boldsymbol{\Omega}'\rightarrow\boldsymbol{\Omega})I_\lambda(\boldsymbol{r},\boldsymbol{\Omega}',t) \quad (3.1)$$

where $I_\lambda(\boldsymbol{r},\boldsymbol{\Omega},t)$ is the spectral radiance (energy/m^2 sr s) of photons at location $\boldsymbol{r}$ traveling in the direction $\boldsymbol{\Omega}=(\mu,\varphi)$ within the cone $d\boldsymbol{\Omega}$. Spectral radiance is the (unknown) physical quantity that describes the light distribution within, entering, and exiting the host medium. Importantly, μ and φ are cosines of the inclination angle and the azimuth angle, respectively, which are used to describe the photons' direction of motion. The two terms on the left-hand side of eq. (3.1) represent net energy loss of photons streaming out of the phase space which is balanced by energy loss due to the scattering and absorption (third term) and the inscattering of photons in the phase space (right-hand side). The participating medium is described by the absorption and scattering coefficients. Here, $\Sigma_{tot}(\boldsymbol{r})$ is the total interaction coefficient, defined as the sum of the absorption and scattering coefficient ($\Sigma_{tot}(\boldsymbol{r})=\Sigma_{abs}(\boldsymbol{r})+\Sigma_{sca}(\boldsymbol{r})$). In addition, $\Sigma_s(\boldsymbol{r},\boldsymbol{\Omega}'\rightarrow\boldsymbol{\Omega})$ is the differential scattering coefficient (also called differential scattering cross section or inscattering coefficient) which describes the probability that photons traveling in the $\boldsymbol{\Omega}'$ direction are scattered in the $d\boldsymbol{\Omega}$ about $\boldsymbol{\Omega}$ direction. In conventional RT theory, the host medium is assumed to be "rotationally invariant" (i.e., the differential scattering coefficient depends only on the angle between $\boldsymbol{\Omega}$ and $\boldsymbol{\Omega}'$). With the latter position, and assuming that the transport of photons is a function of only one spatial variable (depth, τ), it is customary to write the differential scattering as $\Sigma_s(\boldsymbol{\Omega}'\cdot\boldsymbol{\Omega})=\omega_\lambda(\tau)p_\lambda(\tau,\cos\Theta)$ where $\omega_\lambda(\tau)$ and $p_\lambda(\tau,\cos\Theta)$ are the single-scattering albedo and the scattering phase function, respectively, and $\Theta=\cos^{-1}(\boldsymbol{\Omega}'\cdot\boldsymbol{\Omega})$ is the angle between the two directions (see Section 3.2.2 for a more precise definition of both $\omega_\lambda(\tau)$ and $p_\lambda(\tau,\cos\Theta)$).

To complete the mathematical description of the balance of photons interacting with the host medium, proper boundary conditions that account for the radiative flux of photons entering the medium must be provided. Importantly, for the case of ice, snow, debris, and their mixtures, the scattering process does not alter photons' energy (i.e., interaction with the host medium does not shift wavelength). Therefore, photons maintain their energy while changing direction. Eq. (3.1) can then be solved independently at each wavelength to determine the radiative regime of the observed surface. In supraglacial lakes, Raman scattering requires that photons change energy during their interaction process. Consequently, eq. (3.1) must be modified with an additional wavelength-dependent source term that accounts for such effects on overall photon balance (see Section 3.2.3). Bioluminescence is normally absent or negligible and is ignored for glacial lakes.

Eq. (3.1) is an integro-differential whose solution has challenged researchers for decades. In the radiative transfer and particle transport communities, it is known as the linearized Boltzmann equation (LBE) and generally does not have any analytical, closed-form solution. Although eq. (3.1) is the basis for our modeling, several assumptions must be enforced to derive a more manageable form. One immediate simplification comes from the observation that the $1/c$ term factoring the time derivative of $I_\lambda(\boldsymbol{r},\boldsymbol{\Omega},t)$ is smaller than the intensity flux time rate (Davis and Knyazikhin 2005). The latter implies that a steady state is reached almost instantaneously. Indeed, radiative transfer in passive remote-sensing applications is generally modeled as a stationary phenomenon; time-dependent RT problems are considered only when modeling the response of the surface to active pulsed illumination by remote-sensing instruments (e.g., LiDAR).

3.2.1 RT modeling approach for glacier surfaces

Glacier surfaces and supraglacial lakes generally exhibit a complex spatial arrangement of different

materials. Consequently, any RT model should be flexible enough to permit the incorporation of compositional and spatial structure scenarios that are typically found in such environments (e.g., a two-layer arrangement that includes an upper layer of mixed snow and debris overlaying a bottom layer of pure bubbly ice). The natural variability of surface composition and lake suspended debris, however, makes it extremely difficult to develop a comprehensive RT model that is simple (i.e., mathematically tractable), accurate, and computationally inexpensive. Clearly, if a comprehensive description of the optical properties appearing in the LBE is available, one may attempt to directly solve eq. (3.1). While this is in principle possible, the dimensionality of the problem (three positions and two angular variables) coupled with the integro-differential nature of the LBE make it virtually impossible to find accurate and fast solutions. Consequently, the RTE must be simplified.

A closer look at the actual material and particle-size arrangements typically found on glaciers provides the insight that simplified geometries can support rigorous but simplified RTEs to describe the BRDF and spectral albedo. A vertically layered approach implies that radiant intensity depends only on one spatial (optical depth) and two angular variables. The layering assumption is justified by real case examples found in natural glacier environments. For example, Fig. 3.1 depicts monomineralic and monolithologic materials, intimate mixtures, and areal mixtures of materials on the Root and Kennicott Glaciers in the Wrangell Mountains, Alaska. Whether a patch of surface material is effectively monomineralic or monolithologic depends on the scale and the situation. To explain areal mixtures, consider Figs. 3.1(A, B). At the ASTER pixel footprint scale (15 m/pixel for VNIR), the major glaciological features (especially medial moraines and intermoraine lanes of ice, snow, and firn) would be totally resolved and are each optically thick; these materials may be approximated as either pure rock debris or pure medium-grained ice (firn). A MODIS pixel (250 m) would not resolve the individual medial moraines and ice patches; in this case, linear areal mixing models could adequately simulate reflectance. So long as photons do not penetrate through grains far enough to interact with different types of minerals, the reflectance signature of such patch-wise areal mixtures is simply the area-averaged reflectance spectra of the mineral components making up the surface.

Figs. 3.1(C–J) show that more complex situations, not well modeled as areal mixtures, are also common on glaciers. Most glaciers possess broad areas of impure ice stained by small amounts of surficial or intermixed rock grit. As detailed close-up images show (Figs. 3.1(I, J); J being an extreme color stretch of I), the rock grit is so fine that it is optically thin and to some extent is intermixed with ice in the upper few millimeters; this slight debris-laden ice has a structure of massive, clean, coarse crystalline ice overlain by a zone just a couple of millimeters thick where ice is effectively intermixed with fine silicate rock particles. We refer to a homogeneous or random intermixing of two (or more) phases, with one phase having high photon transmittance relative to the other phase, like an intimate mixture. Thus, intimate mixtures permit photons to interact with two or more materials of differing optical properties (e.g., ice with intermixed rock flour). As we demonstrate in the simulation section, such intimately mixed surfaces exhibit unique spectral properties and unique bidirectional reflectance characteristics different from pure ice, pure rock, or areal mixtures of rock and ice.

The glacier surface also has centimeter-scale grit-free ''windows'' that expose the coarse crystalline ''blue ice'', and optically thick centimeter-size rock particles. Photons are admitted through the grit-free windows into coarse-grained massive ice below the gritty ice. The grittier areas admit and emit fewer photons per square millimeter, but they dominate the area fraction of this surface. Although Figs. 3.1(I, J) point out the real world complexity of such surfaces from a radiation transfer perspective, we can approximate the geometry as a deep layer of clean coarse crystalline ice overlain by a thin layer of an intimate mixture of ice with fine rock detritus. The more complex real world geometry can then be simulated by patches of intimately mixed dirty ice with patches of pure clean ice and patches of pure debris. Complex, realistic scenarios can therefore be generated in a stepwise fashion.

The layering assumption reduces the dimension of the RTE yet allows meaningful modeling of a wide range of spatially complex material structures, including multi-layers of intimate mixtures. In this framework, two major configurations for material arrangement are possible. In the first configuration, intimate mixtures of ice and sediment can be modeled as a homogeneous single layer (optically thick), where the optical properties of the layer are derived by a weighted average of the optical properties of the pure components (see Section 3.3.4). In the sec-

Figure 3.1. (A–J) Examples of monomineralic and monolithologic materials, intimate mixtures, and areal mixtures of materials on the Root and Kennicott Glaciers in the Wrangell Mountains, Alaska. On the right side of the figure are illustrated a set of typical scenarios that can be modeled using multi-layer 1 D, two-angle radiative transfer equations (eq. 3.3). The geometrical configurations include single-layer and multi-layer arrangements of mixtures of ice and rock debris. Figure can also be viewed as Online Supplement 3.1.

ond configuration, the surface is assumed to exhibit an idealized multi-layer structure. Each layer is modeled as homogeneous, with a defined optical thickness, and its composition may include either a pure material or an intimate mixture of different elements (ice, snow, debris). In addition, RT models should be able to describe scenarios where, in a single-layer configuration, the surface exhibits patches of homogeneous material. Within the limits of its spatial resolution, any remote-sensing instrument measures the spectrally average electromagnetic radiation reflected by the area corresponding to one pixel. Assuming an independent pixel approximation (IPA), RT models can be devised to compute the flux intensity of heterogeneous patched areas by calculating the average flux intensity of homogeneous subpixel components weighted with their area coverage.

3.2.2 Radiative transfer equation in layered mixtures of snow, ice, and debris

The major assumption that reduces the problem dimension is to set the medium to be infinite in the horizontal direction so that photon transport within the medium is one dimensional (the depth variable). If a single-layer configuration is considered, a further simplification is obtained by working with a spatially homogeneous medium. Vertical heterogeneity can be described by assuming a multi-layer configuration where the medium is subdivided in many layers, each having different optical properties. Under these conditions, the LBE can be simplified. The spectral radiant intensity for a vertically heterogeneous medium is governed by the following 1D, two-angle RTE (Chandrasekhar

1960, Siewert 1978, 2000):

$$\mu\frac{\partial}{\partial\tau}I_\lambda(\tau,\mu,\varphi)+I_\lambda(\tau,\mu,\varphi)=\frac{\omega_\lambda(\tau)}{4\pi}\int_0^{2\pi}d\varphi'\int_{-1}^{1}d\mu'\,p_\lambda(\tau,\cos\Theta)I_\lambda(\tau,\mu',\varphi') \tag{3.2}$$

where, for a given wavelength λ, $I_\lambda(\tau,\mu,\varphi)$ is the spectral radiant intensity, $\tau=\int_0^x\sigma_{tot}\,dx'$ is the optical thickness (varying in the range $\tau\in[0,\Delta]$), $\mu\in[-1,1]$ is the cosine of the polar angle (measured from the positive τ-axis), $\varphi\in[0,2\pi]$ is the azimuth angle, $\omega_\lambda(\tau)=\sigma_{sca}(\tau,\lambda)/\sigma_{abs}(\tau,\lambda)$ is the spatially dependent single-scattering albedo, defined as the ratio between scattering coefficient $\sigma_{sca}(\tau,\lambda)$ and total interaction (extinction) coefficient ($\sigma_{tot}(\tau,\lambda)=\sigma_{sca}(\tau,\lambda)+\sigma_{abs}(\tau,\lambda)$ (i.e., sum of absorption and scattering coefficient), and $p_\lambda(\tau,\cos\Theta)$ is the spatially dependent scattering phase function.

In the case of a multi-layer approximation, the medium is subdivided into N layers each having different optical properties. For each layer, the single-scattering albedo and the scattering phase function are defined either for a single material or for a mixture, respectively as ω_λ^s, $s=1,\ldots,N$ and $p_\lambda^s(\cos\Theta)$, $s=1,\ldots,N$. For each of the N layers, we write the following equation ($s=1,\ldots,N$):

$$\mu\frac{\partial}{\partial\tau}I_\lambda^{(s)}(\tau,\mu,\varphi)+I_\lambda^{(s)}(\tau,\mu,\varphi)=\frac{\omega_\lambda^{(s)}}{4\pi}\int_0^{2\pi}d\varphi'\int_0^{2\pi}d\mu'\,p_\lambda^{(s)}(\cos\Theta)I_\lambda^{s}(\tau,\mu',\varphi') \tag{3.3}$$

The RTE must be equipped with boundary conditions describing radiant intensity at the top and bottom layers. Moreover, the continuity of radiance between layers must be enforced. For $s=1$ (top boundary condition):

$$I_\lambda^{(1)}(0,\mu,\varphi)=S_0\delta(\mu-\mu_0)\delta(\varphi-\varphi_0)+f(\mu,\varphi) \tag{3.4}$$

At the interface between slabs:

$$\left.\begin{aligned}I_\lambda^{(s)}(\tau^{(s)},\mu,\varphi)&=I_\lambda^{(s-1)}(\tau^{(s)},\mu,\varphi)\\ I_\lambda^{(s)}(\tau^{(s+1)},\mu,\varphi)&=I_\lambda^{(s+1)}(\tau^{(s+1)},\mu,\varphi)\end{aligned}\right\} \tag{3.5}$$

For $s=N$ (bottom-boundary condition):

$$I_\lambda^{(N)}(0,-\mu,\varphi)=0 \tag{3.6}$$

where $\mu\in[0,1]$. Eq. (3.4) represents the incident directional field (first term on the RHS) and diffuse radiation field (second term at the RHS). Eq. (3.5) ensures that the continuity of radiant intensity at the interface between layers is respected. Eq. (3.6) imposes a non-reentrant boundary condition at the bottom layer. Typically, the bottom layer is assumed to be optically thick (i.e., semi-infinite).

3.2.3 Radiative transfer equation in glacier lake waters

RT modeling for glacier-related surface water can be based on using a plane-parallel approximation, where the water column is assumed to be layered, and surface irradiance is assumed to be uniform over the surface. Because of small horizontal variation in water optical properties, the RT problem can be treated spatially using the depth variable. Using notation that is customary in the ocean optics community, radiance is governed by the following integro-differential equation:

$$\mu\frac{\partial}{\partial z}L(z,\mu,\varphi,\lambda)+c(z,\lambda)L(z,\mu,\varphi,\lambda)=b(z,\lambda)\int_0^{2\pi}d\varphi'\int_{-1}^{1}d\mu'\,\beta(z,\mu'\to\mu,\varphi'\to\varphi,\lambda)\times L(z,\mu',\varphi',\lambda)+S(z,\lambda), \tag{3.7}$$

where z is downward distance from the lake surface, μ is the cosine of the polar angle, and φ is the azimuth angle in the horizontal plane. The sum of the scattering and absorption coefficient is called the beam attenuation (extinction) coefficient $c(z,\lambda)=a(z,\lambda)+b(z,\lambda)$, whereas $\beta(z,\mu'\to\mu,\varphi'\to\varphi,\lambda)$ is the scattering phase function. Properties $a(z,\lambda)$, $b(z,\lambda)$, and $c(z,\lambda)$ are commonly known as inherent optical properties (IOPs). IOPs are critical parameters that describe the bulk optical behavior of lake water and are of general interest in inverse remote sensing. $S(z,\lambda)$ is a source function that accounts for the Raman scattering phenomenon. Such a term complicates the nature of the equation, and finding accurate numerical solutions becomes more challenging. This is due to the fact that in such cases the problem cannot be solved "one wavelength at a time" as in the conventional case (see Section 3.2.2). The latter implies that in eq. (3.7), the wavelength variable is coupled with both spatial and angular variables. Nevertheless, a simplified version of eq. (3.7) which does not depend on $S(z,\lambda)$ may be sufficient to describe photons' behavior because bioluminescence sources are very small during the daytime, and both fluorescence and Raman scattering become negligible.

Glacier lake water is generally assumed to be either homogenous (well mixed) or vertically stratified which, as in the case for glacier surfaces, enables the use of multi-layer configuration models. Eq. (3.7) is also equipped with boundary conditions that are similar to the one described in the previous section. The top layer is illuminated by an incident and diffuse source (see eq. 3.4). If lake depth is large, the medium is optically thick and non-reentrant conditions at the bottom layer (eq. 3.6) are appropriate. If the lake is shallow, reflective boundary conditions, which depend on lake bottom composition, shall be imposed at the bottom layer, although we do not provide simulations of such instances.

3.3 OPTICAL PROPERTIES OF SNOW, ICE, DEBRIS, MIXTURES, AND GLACIER LAKE WATER

The RTE can be solved as a function of surface/water properties (e.g., mineralogical composition, grain size distribution) and solar/sensor geometry. The RTE describes the multiple scattering of photons through the host medium and critically depends on single-particle optical behavior. From the photon–medium interaction point of view, such behavior is regulated by the ability of the host medium to absorb and scatter light in any direction. Indeed, a single particle is characterized by absorption and scattering efficiencies that are related to the probability that a photon will be scattered or absorbed by a single particle of defined shape and size. Scattering and absorption processes are accounted for via two optical property parameters: (1) single-scattering albedo, which represents the probability of a single photon to be scattered in any direction; and (2) the scattering phase function $p_\lambda(\cos\Theta)$ (or $\beta(z,\mu'\rightarrow\mu,\varphi'\rightarrow\varphi,\lambda)$ for glacier lake water), with Θ being the angle between the incident and scattering direction. The phase function specifically describes the probability that a photon coming from a direction $\mathbf{\Omega}'=(\mu',\varphi')$ is scattered by a particle in direction $\mathbf{\Omega}=(\mu,\varphi)$. Particulates that typically comprise surfaces in glacier environments are rotationally invariant (i.e., the probability of scattering depends only on the relative angle between incident and scattered radiation). While single-scattering albedo is a scalar parameter ranging between 0 and 1, the phase function is customarily described by a series of coefficients representing the projection of $p_\lambda(\cos\Theta)$ on Legendre polynomials. Generally, snow, ice, soil, and water exhibit a strongly forward-peaked scattering function (i.e., relatively large single particles tend to scatter radiation primarily in the forward direction). The latter implies that a large number of coefficients (of the order of thousands) are required to accurately characterize the single-particle phase function. The asymmetry parameter g, which is defined as the cosine of the average of $p_\lambda(\cos\Theta)$ (also as the degree of forward scattering of the medium), may be conveniently employed to reduce the number of parameters required to describe the optical properties of a single particle. The popular Heyney–Greenstein model is therefore widely used to approximate the phase function for the particles of interest:

$$p(\cos\Theta)=\frac{1-g^2}{(1-2g\cos\Theta+g^2)^{3/2}},\quad g\in[-1,1] \tag{3.8}$$

The scattering phase function can be expanded in Legendre polynomials $P_l(\cos\Theta)$ with coefficients that are directly related to the asymmetry parameter in the following manner:

$$p(\cos\Theta)=\sum_{l=1}^{L}\beta_l P_l(\cos\Theta) \tag{3.9}$$

$$\beta_l=(2j+1)g^l \tag{3.10}$$

Therefore, single-particle optical properties can be, at minimum, characterized by knowledge of single-scattering albedo and asymmetry parameter. Alternatively, a number of scattering coefficients are required to describe the particle phase function. Such parameters depend on the size of the particle, wavelength, index of refraction, and the shape of the particle. The most common approach to determine optical properties is to assume that the particle is a perfect sphere. In this case, optical properties can be computed in closed form by directly solving Maxwell equations. Mie theory (Wiscombe 1980) has been widely used to model the optical properties of snow, ice, and soil. More involved approaches, such as the T-matrix method (Watermann 1971, Mackowski and Mishchenko 1996) and the ray-tracing method (Bohren and Barkstrom 1974, Macke et al. 1996), have been developed to account for arbitrary and irregular shapes. Such methods, however, tend to be computationally expensive.

3.3.1 Snow

From the radiative transfer perspective, snow can be viewed as a collection of ice particles immersed in air. A single particle of ice has variable shape and size and an exact description of single-scattering albedo and phase function involves using methods of geometric optics. Yang and Liou (1998) applied Monte Carlo–driven ray-tracing algorithms to compute the optical properties of ice crystals for a substantial variety of shapes including plates, hollow columns, bullet rosettes, and ice aggregates. Whereas a database of properties has been generated, accurate description of the phase function for such complex shapes implies that one needs RT code capable of handling thousands of phase function coefficients to compute the radiative regime in media with irregular particles, which results in impractical computationally expensive calculations. A more popular approach employed to describe snow particle optical properties makes extensive use of Mie-based code. Founded on Mie theory (Wiscombe 1980, 1996), such code can effectively compute efficiencies, single-scattering albedo, and asymmetry parameters as a function of grain size. However, calculations based on Mie theory may be severely limited by the fact that the theory works rigorously only if the particles are assumed to be perfect spheres. Whereas single snow particles are not spheres, an ensemble of snow particles is postulated to behave as "optically equivalent spheres" (i.e., a collection of snow grains having the same volume/surface ratio; Dozier et al. 1987). Mugnai and Wiscombe (1980) demonstrated that a collection of nonoriented spheroids have the same scattering behavior as an ensemble of spherical particles of equivalent size. Mie-based code requires knowledge of the complex index of refraction $n = n_r + n_i$. Generally, the real part is interpreted as phase velocity and the imaginary part describes absorption loss for an electromagnetic wave moving through the particle. For the case of ice, the imaginary part is linked to volume absorption of ice (Wiscombe and Warren 1980). Fig. 3.2 shows both real and imaginary parts of the index of refraction for pure ice (Wiscombe 1980, Warren and Brandt 2008). Importantly, the magnitude of the imaginary part varies across the visible and the near-infrared (NIR) by many orders of magnitude implying that: (1) ice is transparent in the visible region (small imaginary index of refraction); and (2) ice is moderately absorptive in the NIR (imaginary index of refraction is larger and

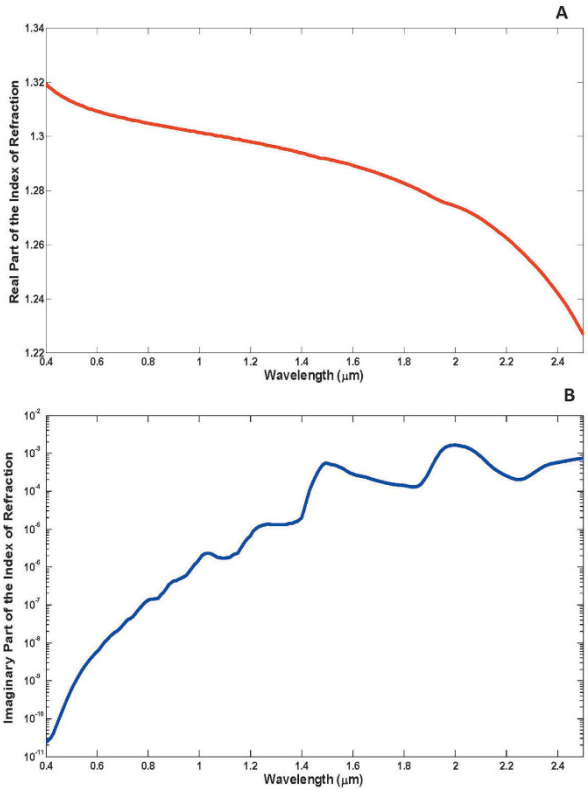

Figure 3.2. Spectral behavior of the real part (A) and imaginary part (B) of the complex index of refraction for pure ice. Figure can also be viewed as Online Supplement 3.2.

increases with wavelength). Wiscombe and Warren (1980) studied the behavior of pure ice single-particle optical parameters using Mie theory and showed that the extinction coefficient and asymmetry parameter are relatively insensitive to wavelength (typical value for g ranges between 0.88 and 1), and that ω_λ (or the co-albedo $1 - \omega_\lambda$) is mainly responsible for the spectral variation of snow albedo. Generally, ω_λ is very close to 1 in the optical region (highly scattering snow medium across the visible) and decreases monotonically reaching a minimum value of 0.5 in the NIR. Increasing grain size is shown to decrease ω_λ. Generally, values of 50 μm are assumed for fresh snow, whereas 1 mm is assumed for grain clusters or wet snow. Water in the snowpack is not usually modeled, as the index of refraction of water is very close to that of ice.

3.3.2 Glacier ice

Whereas snow and ice are the major material components, the physical state and the optical proper-

ties of various glacier surface characteristics under investigation vary dramatically. Snowfall is transformed to ice through a variety of mechanisms including: (1) mechanical settling; (2) sintering; (3) refreezing of meltwater; and (4) refreezing of sublimating ice. The grain size of surface ice varies widely. In the accumulation zone, fine snow may dominate. In the firn zone (annealed snow), grain size may effectively be in the range of several millimeters. In the ablation zone, bubbly ice may have an effective grain size of a few millimeters, but dense, well-crystallized ice may have grain sizes of 1–10 cm. In some cases, glaciers may be effectively layered in the optical zone, with a dusting of snow or bubbly ice overlying denser, coarser ice. Multiple scattering of such complex structures requires proper modeling of the properties of single components which are usually mixed with other components (snow, bubbles, rock debris, and soot, see Section 3.3.4) and possibly arranged in multi-layer configurations. However, glacier clean ice may be modeled as a collection of bubbles trapped within a matrix of transparent ice.

The firn, which is snow material after the transformation process has begun, is initially porous and contains interconnected air channels. As the density increases above 880 kg/m^3, the channels close off resulting in a mixture of ice and bubbles trapped within the glacier body. Mullen and Warren (1988) provided a framework for modeling the volumetric scattering of such bubbly ice. Indeed, in a pure ice sample containing only air bubbles, the physics of interaction between the photons and the host medium is such that absorption occurs in the ice matrix and scattering occurs at ice bubble boundaries. Thus, the absorption process is generally separated from the scattering process. Scattering is dominated by the size and distribution of the air bubbles within the ice. If bubbles are assumed to be spheres, Mie theory can be employed to compute the scattering efficiency (and subsequently the scattering coefficient) as well as the asymmetry parameter as a function of bubble size. In this case, the Mie-based calculation follows the same process as in the case of snow, but with the imaginary part of the complex of refraction set to zero ($n = n_r$). Marston et al. (1982) found good agreement with the scattering of a single air bubble in water, which has an index of refraction similar to ice. Conversely, absorption is assumed to be exclusively a function of the amount of ice per unit volume. For example, Bohren (1983) assumed that the absorption coefficient of an air–ice mixture is that of pure ice multiplied by the volume fraction of ice in the sample. Once the scattering and absorption coefficients are available, both the extinction coefficient and single-scattering albedo can be computed to complete the optical characterization of the volumetric scattering of clean ice.

Microtopography is important on some glacier surfaces and can introduce complex scattering and microshadowing effects. We do not address this important topic in this chapter.

3.3.3 Rock debris

Debris-covered glaciers include varying amounts, grain sizes, and spatial arrangements of rock debris. Moraines may consist mainly of boulders and cover the ice completely. Debris patches may be scattered amongst clean ice exposures. Fine rock flour may be intimately mixed with ice. The optical characterization of single-particle absorption and scattering for soil/sediment is, however, very difficult. Generally, soil particle distributions can vary in size, shape, and mineralogy. Whereas Mie theory has been fairly successful in describing the optical properties of snow and ice, it has not been able to accurately reproduce the optical properties of soil particles. Indeed most materials found on Earth and planetary surfaces exhibit a nonuniform structure and composition.

Two decades ago, Hapke (1993) presented a generalized model for the scattering efficiency of large irregular particles. The model is based on an extension/generalization of the equivalent slab model for irregular particles. The model is approximate but can be used to compute scattering efficiency in closed analytical form and has been mostly employed in the planetary science community (e.g., Warell et al. 2009). More recently, T-matrix code has been made available to describe the optical properties of particles that are large and irregular. Based on the linearity of Maxwell's equations (Watermann 1971), the method has some computational advantage where the particle under consideration is axial symmetric, because the matrix is easily subdivided into independent matrices, yielding more efficient and faster calculations. T-matrix methods are also available to compute the optical properties of particle clusters with defined orientation (Mackowski and Mishchenko 1996). Generally, such algorithms are computationally expensive, and recently some of the available code has been redesigned to run on parallel clusters of machines (Mackowski and Mishchenko 2011).

3.3.4 Mixtures

The optical properties of single particles can be employed to determine the optical behavior of multicomponent mixtures. Computing single-scattering albedo and the asymmetry parameter for a mixture is fairly straightforward. Let us consider the case of two pure components each characterized by spherical particles of radius r_1 and r_2 and with scattering coefficient $\sigma_{sca,1(2)} = n_{1(2)}\pi r_{1(2)}^2 Q_{sca,1(2)}$ and total interaction (extinction) coefficient $\sigma_{tot,1(2)} = n_{1(2)}\pi r_{1(2)}^2 Q_{tot,1(2)}$ where $Q_{sca,1-2}$ and $Q_{tot,1-2}$ are the scattering and extinction efficiencies for type 1(2) particles, and $n_{1(2)}$ is the number of particles per unit volume of type 1(2) particles. The combined single-scattering albedo of a mixture of two types of particles can be determined as follows:

$$\omega_{mix} = \frac{\sigma_{sca,1} + \sigma_{sca,2}}{\sigma_{tot,1} + \sigma_{tot,2}} = \frac{n_1\pi r_1^2 Q_{sca,1} + n_2\pi r_2^2 Q_{sca,2}}{n_1\pi r_1^2 Q_{tot,1} + n_2\pi r_2^2 Q_{tot,2}} \tag{3.11}$$

If particles are not spherical, πr^2 shall be replaced by relative particle cross-sectional area. If particle size is modeled as a size distribution, then computing an integral with the weighted size distribution is required. Similarly, combined phase function moments are computed by averaging the moment of each component and weighting it by its scattering coefficient. For example, the asymmetry parameter of a two-component mixture is computed as follows:

$$g_{mix} = \frac{g_1\sigma_{sca,1} + g_2\sigma_{sca,2}}{\sigma_{sca,1} + \sigma_{sca,2}} = \frac{g_1 n_1\pi r_1^2 Q_{sca,1} + g_2 n_2\pi r_2^2 Q_{sca,2}}{n_1\pi r_1^2 Q_{sca,1} + n_2\pi r_2^2 Q_{sca,2}} \tag{3.12}$$

3.3.5 Glacier lake water

Glacier water includes lakes, streams, and small puddles and rivulets. In this section we will not consider thin films (such as wetted rocks and water-saturated snow) or optically thin ponds where substrate effects are important. The optical properties of optically thick glacier water are described by explicitly characterizing the absorption, scattering, and total beam attenuation coefficients as a function of the various components present in the water body. Optical properties are responsible for the large variation in the supraglacial lake colors that can be observed in alpine environments ranging from exquisite turquoise and other pastels, to brilliant green, cobalt blue, and gray. The colors of optically deep lakes pertain mainly to their suspended sediment loads, especially clastic sediment in glacial lakes and substrate effects for optically shallow lakes.

Suspended clastics in glacier meltwater have two major components: (1) rock flour—mainly clay to fine silt size—produced by glacier grinding at the bed; (2) silt and sand introduced by nonglacial streams and incorporated into glacier waters from mass-wasting deposits or other sources that have not been pulverized at the glacier bed. These components are usually distinct in their grain-rounding, faceting, and particle size–frequency distributions. In heavily glacierized basins (where glacial sediment input is much greater than nonglacial input) in nonpolar climates (where glaciers have thawed beds), glacier rock flour overwhelmingly dominates most lakes. Glacial grinding produces extremely fine particles due to rock being forced to slide over other rocks, whereas in ordinary streams, particles are generated as chips that are shed from larger clasts during water-driven impacts. The energy and momentum relations are such that particles a few microns in radius become ineffective abrading agents in normal streams. Hence, glacial rock flour includes particles sizes from hundreds of microns to a tenth of a micron or smaller, whereas non-glacial streams normally carry suspended load particle sizes from a few hundred microns down to a few microns. Although particle sizes on the scale of light wavelengths can total up to a small fraction of the total mass of suspended load, those size ranges can dominate scattering due to the large specific surface area of those fine grains. Such particle sizes can be virtually absent from nonglacial waters, thus accounting for some of the difference between the colors of typical nonglacial lakes versus glacial lakes.

From the optical perspective, turbid nonglacial lake waters, which are generally classified as "Case 2" waters (Mobley 1994), can be difficult to characterize because they often consist of water plus dissolved organic and inorganic matter. Most glacial lakes and streams have negligible organic components, but some isolated ponds can develop a biota and suspended and dissolved organic matter. These lakes are strongly influenced by colored dissolved organic matter (CDOM also known as Gelbstoff, yellow substance, or gilvin), detritus, mineral particles, bubbles, and other substances including phytoplankton. Such particles are not

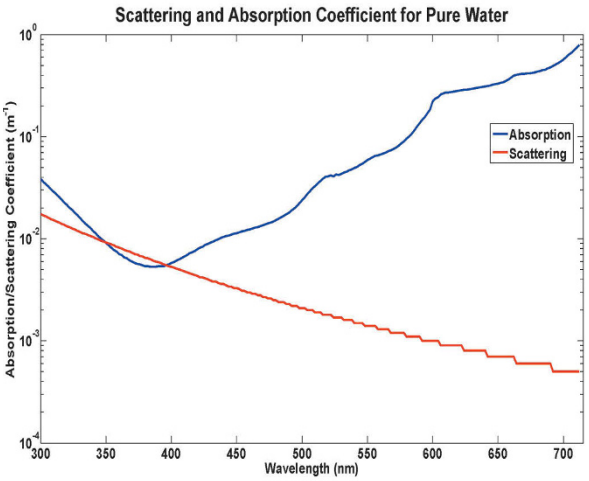

Figure 3.3. Spectral behavior of absorption and scattering coefficients for pure water. Figure can also be viewed as Online Supplement 3.3.

very well characterized in terms of type and location, and they do not covary with phytoplankton concentration as in Case 1 waters. Generally, the optical properties of such waters are assumed to be additive, where the absorption and scattering coefficient can be written as a sum of the models employed for absorption and scattering of the individual components:

$$a(\lambda) = a_W(\lambda) + a_P(\lambda) + a_X(\lambda) + a_Y(\lambda) \quad (3.13)$$

$$b(\lambda) = b_W(\lambda) + b_P(\lambda) + b_X(\lambda) + b_Y(\lambda) \quad (3.14)$$

where $a_W(\lambda), a_P(\lambda), a_X(\lambda), a_Y(\lambda)$ $(b_W(\lambda), b_P(\lambda), b_X(\lambda), b_Y(\lambda))$ are the absorption (scattering) coefficients for pure water, phytoplankton, mineral particles/detritus, and CDOM, respectively. Models and/or experimental data for individual components are more or less available. For pure water, scattering and absorption coefficients have been measured. Fig. 3.3 shows the wavelength-dependent scattering and absorption coefficient of pure water as measured by Pope and Fry (1997). Optical models for phytoplankton and CDOM are available from the literature (Prieur and Sathyendranath 1981). Generally, CDOM absorption is assumed to decay exponentially with wavelength, whereas scattering due to dissolved microscopic pigments is assumed to be negligible. Phytoplankton absorption is a complex function of its concentration and wavelength, and requires two empirical wavelength-dependent functions. Phytoplankton scattering is proportional to the inverse of the wavelength and directly proportional to its concentration to the power of 0.6. Suspended particle optical properties in glacier lakes are not well known and require in situ measurement. Suspended sediments tend to be mostly scatterers although iron-rich sediments may exhibit strong absorption features. Heege (2000) measured the optical behavior of suspended particles in Lake Constance and found that the particles had no influence on the overall absorption coefficient ($a_X(\lambda) = 0$) whereas they heavily influenced the scattering properties of the lake waters. It was found that the backscattering coefficient was independent of wavelength and proportional to the particle concentration.

Scattering in glacier and oceanic environments is strongly forward peaked with peak ratio between forward and backward single-scattering ratios of the order of 10^5. Various models are available to describe such a type of scattering behavior although two types of phase functions are generally used for water including the Petzold phase function (Petzold 1972) and the Fournier–Fourand model (Fournier and Fourand 1994). Mobley et al. (2002) examined the effect of various phase functions on the computed radiance and concluded that: (1) knowledge of the appropriate phase function is as important as knowledge of the absorption and scattering coefficient; and (2) accurate knowledge of the shape of the phase function is not required as long as the backscattering fraction is correct. It was also shown that the Fournier–Fourand model works very well.

3.4 NUMERICAL SOLUTION OF THE RTE

Computing the radiative regime within glaciers, as well as the amount of radiation reflected by glacier surfaces and/or glacier lakes, requires solving the RTEs formally presented in the previous sections. Due to its mathematical complexity, an analytical description of the light field is virtually impossible. Over the past few years, many approximate methods have been developed to provide analytical expressions for the multiple scattering of photons in snow, ice, and soil. One of the most popular analytical methods is based on approximating the radiance as one upwelling and one downwelling stream of photons as they are constrained to move only in two directions (two-stream approximation).

Such an assumption allows the determination of analytical formulas that quickly compute upwelling and downwelling diffuse fields (see Wiscombe and Warren 1980 for an example of a two-stream calculation applied to the problem of determining snow albedo). In an attempt to provide a quantitative tool for the analysis and interpretation of the light reflected by planetary surfaces, Hapke (1981) determined an analytical expression for the reflectance factor of an optically thick surface. He decomposed the radiative field into two major components consisting of a scattered component and a multiple-scattered component. An approximate solution was obtained by: (1) determining an exact expression for the first scattered component; and (2) determining an approximate analytical expression for the multiple-scattered component, assuming that the host medium is isotropic from the second collision on.

Whereas approximate methods provide the analyst with analytical expressions that are easy to implement, they do not provide accurate solutions of the RTE. Indeed, accurate solutions can be found only by solving the RTE numerically. Over the past two decades, the widespread availability of high-speed digital computers permitted researchers to develop and test more efficient and faster algorithms to compute radiance and the reflectance factor. All the available numerical algorithms have been based on some form of discretization of the spatial and angular variable, thus resulting in RT software that can be used to simulate the light reflected by various surfaces.

One of the most efficient ways to solve the RTE is to discretize the angular variable in a set of finite directions, and then solve the resulting differential equations. Cast as an eigenvalue problem, the set of equations can be solved using conventional numerical methods (e.g., relaxation method) to find an analytical expression for radiance along fixed directions. The DISORT code (Stamnes et al. 1988) is the most popular and is based on discretizing the angular variable. It has been widely used by the community to compute the reflectance factor and spectral albedo of snow as a function of grain size (e.g., Aoki et al. 2000, Painter et al. 2003).

Recently, Siewert (2000) proposed a new formulation of the discrete ordinate approach for a single layer with specified optical properties and thickness. The method, called the analytical discrete ordinates method (ADO), is a novel semi-analytic approach in which the angular variable is discretized to determine a set of ordinary differential equations that have unknown radiant intensities along discrete directions. The set of equations are solved by: (1) numerically solving the resulting eigenvalue problem to compute the homogeneous solution; and (2) use of a modified Green's function formulation to compute the particular solution of the set of differential equations arising from angular discretization. More recently, the method has been extended to include multiple layers of optical properties with special routines that give the method the ability to quickly and efficiently handle thousands of layers (Picca et al. 2007, 2008a, Picca 2009, Previti 2010, Previti et al. 2011). The principles behind the ADO have been implemented in a novel RT code called Multi-layer Analytical Discrete Ordinates Code (MADOC, Furfaro et al. 2014). Developed in a MATLAB environment, MADOC will be soon made available to the larger scientific community. Importantly, MADOC was used to provide the simulation examples in the next section. Discrete ordinate methods have also been used to generate code capable of computing matter/energy interactions in water. Indeed, the Coupled Ocean Atmosphere Radiative Transfer code (COART; Jin et al. 2006) extended the DISORT numerical platform to handle the change in photon direction between the water and atmosphere interface due to differences in the index of refraction.

In principle, both angular and spatial variables can be discretized to transform the RTE into a set of differential equations that can be implemented using a digital computer. The most elementary approach to what is called "vanilla discretization" is the SN[1] method (Lewis and Miller 1984). One major drawback of the method is that accurate solutions can only be obtained if the discretization mesh is sufficiently fine. For optically thick media and settings with forward-peaked phase functions, the method becomes computationally expensive. More recently, it has been shown that accurate solutions of the RT equation can be obtained by solving a sequence of RT problems using SN from coarser to finer grids and coupled with acceleration techniques to find the mesh-independent limit (Ganapol and Furfaro 2008).

Two other alternative methods are suitable for RT calculations involving particulate media. The "adding–doubling method" (Hansen and Travis 1974) is based on the idea that the medium is sliced in thin layers with light entering the top layer. The angular reflectance (and transmittance) of the com-

[1] SN is the codeword for discrete ordinates method.

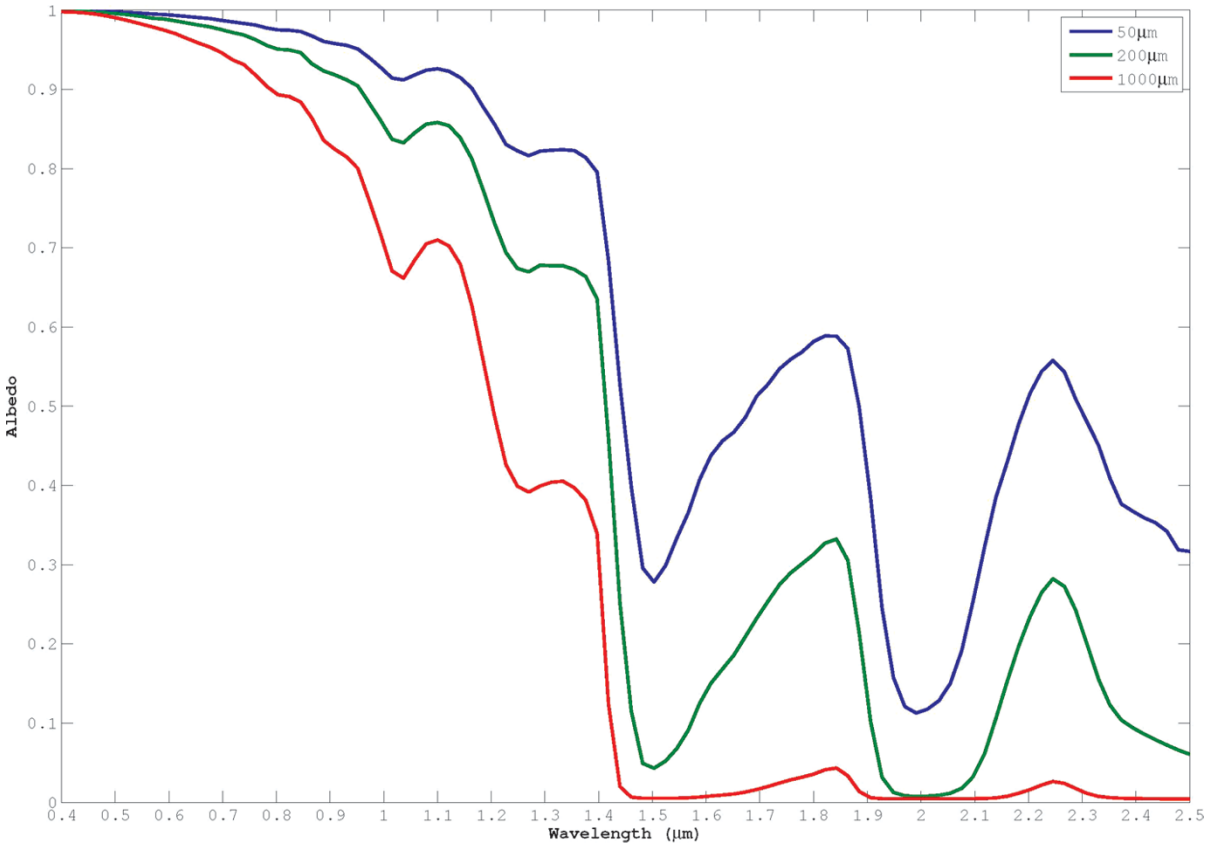

Figure 3.4. RT-based model of spectral albedo for a layer of optically thick pure snow as a function of wavelength (0.4–2.5 μm) and grain size (50, 200, and 1,000 μm). The solar zenith angle is 30°. Compare with Figure 2.8 (Bishop et al.'s chapter). Figure can also be viewed as Online Supplement 3.4.

bined layers is obtained by superposing the reflectance and transmittance of the individual layers. The adding–doubling model has been implemented by de Hann et al. (1987). Another efficient RT model devised to compute the bidirectional reflectance factor of an optically thick surface of particulate media (including snow, ice, debris, and mixtures) was implemented by Mishchenko et al. (1999). The method is based on iteratively solving a nonlinear integral equation (an Ambartsumian equation) derived from photon conservation. The method is efficient because it does not need to solve for light inside the medium and may be ideal for modeling reflected radiance.

Finally, the light field in water can be computed using a commercially available program called HYDROLIGHT (Mobley 1994). Written in Fortran, the code uses the invariant-embedding approach to solve eq. (3.7) for each of the azimuthal components. It has an extensive library of optical properties, and may be purchased for a fee.

3.5 GLACIER RADIATIVE TRANSFER SIMULATION EXAMPLES

Proper modeling of the BRF and spectral albedo based upon surface properties requires solving the RTE as presented in eqs. (3.3) and (3.7). Here, we recall their definitions (see Chapter 2 of this book by Bishop et al.). The bidirectional reflectance factor (BRF) represents the ratio between the radiance emitted in any particular direction by the surface, and the radiance that would be reflected into the same direction given an ideal Lambertian surface, illuminated by the same incident geometry. Conversely, the spectral albedo of a surface is a dimensionless ratio of the radiant energy scattered away from the surface to that received by the surface at a specified wavelength. In this section, a set of numerical examples that show how RT theory can be employed to model BRF and spectral albedo for a variety of configurations typically found in alpine glaciers and glacier lakes are presented. The

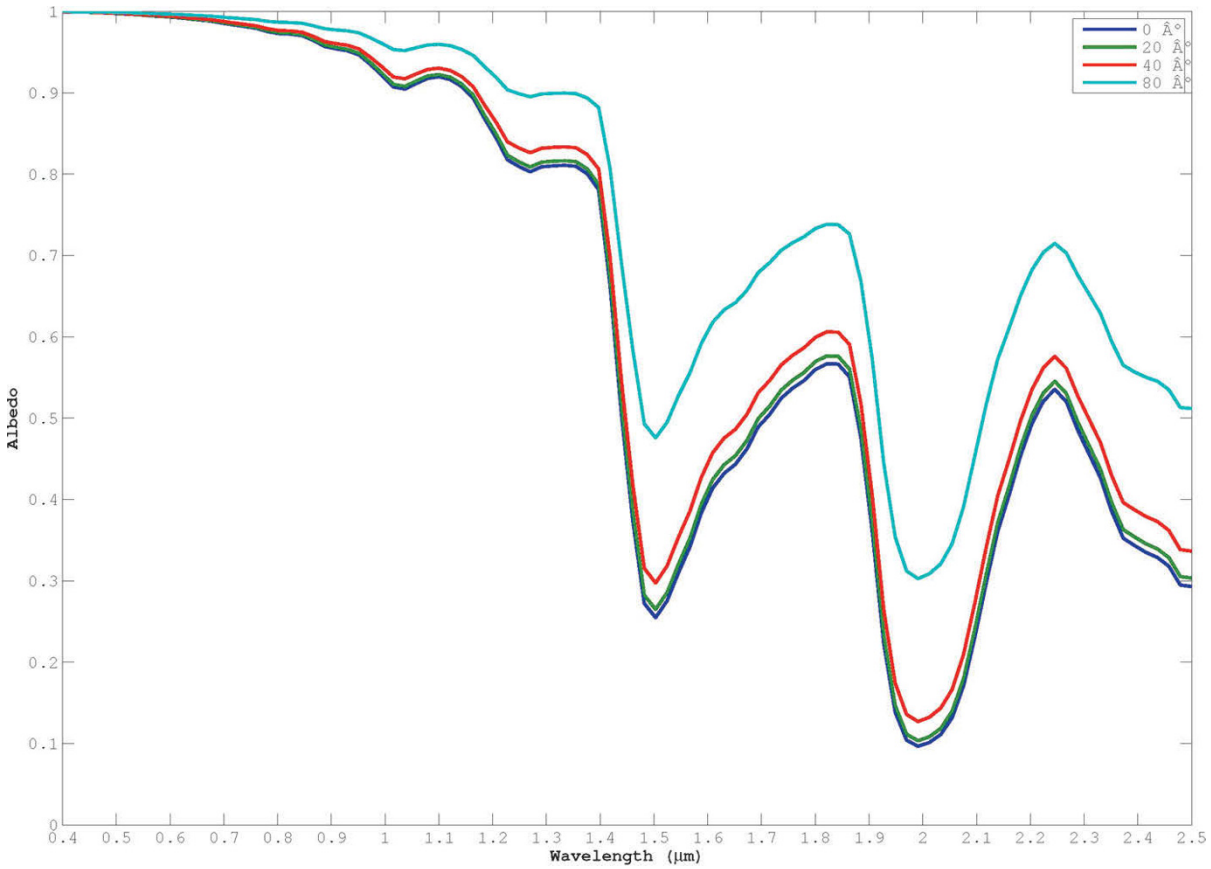

Figure 3.5. RT-based model of spectral albedo for a layer of optically thick pure snow as a function of wavelength and solar zenith angle. The particle grain size is fixed and assumed to be 50 μm. Figure can also be viewed as Online Supplement 3.5.

MADOC platform (Previti 2010, Previti et al. 2011, Furfaro et al. 2014) has been employed in all simulations involving glacier surfaces. Conversely, parameterization of HYDROLIGHT, as presented by Albert and Mobley (2003), has been employed to model reflectance factors for glacier lake scenarios.

In the first set of simulations, RT theory has been employed to model the spectral albedo of a layer of optically thick pure snow as a function of wavelength (0.4–2.5 μm) and grain size (Fig. 3.4). The solar zenith angle was set at 30°. The single-particle optical properties of single-scattering albedo and asymmetry parameter, were computed using the MATLAB-based Mie code provided by Matzler (2004). The ice complex index of refraction was used as input and grain sizes of 50 μm (fresh fine snow), 200 μm (fresh coarse snow) and 1 mm (annealed snow; i.e., firn) were considered.

As shown in Fig. 3.4, albedo is very sensitive to grain size and decreases as the radius of the snow particle increases. From the physical point view, photons have higher chances to be scattered at the boundary between fine snow grains and air. Incrementally larger grain size has the effect of increasing the mean free path, giving photons a higher chance to travel through the ice, and a smaller chance to be scattered and exit the snowpack. Whereas larger snow particles are both more absorptive and more forward scattering, it can be shown that the decrease in albedo is mainly due to the fall of ω_λ in the NIR regime, where the asymmetry parameter increases only slightly (Wiscombe and Warren 1980). Importantly, in the visible region of the spectrum, snow particles are highly scattering (ω_λ very close to one), which explains why snow has generally such a high albedo, independent of grain size.

In the second set of simulations, a RT model was employed to compute the spectral albedo of a layer of optically thick pure snow as a function of wavelength (0.4–2.5 μm) and solar zenith angle (Fig. 3.5). Grain size was fixed and assumed to be 50 μm. Mie

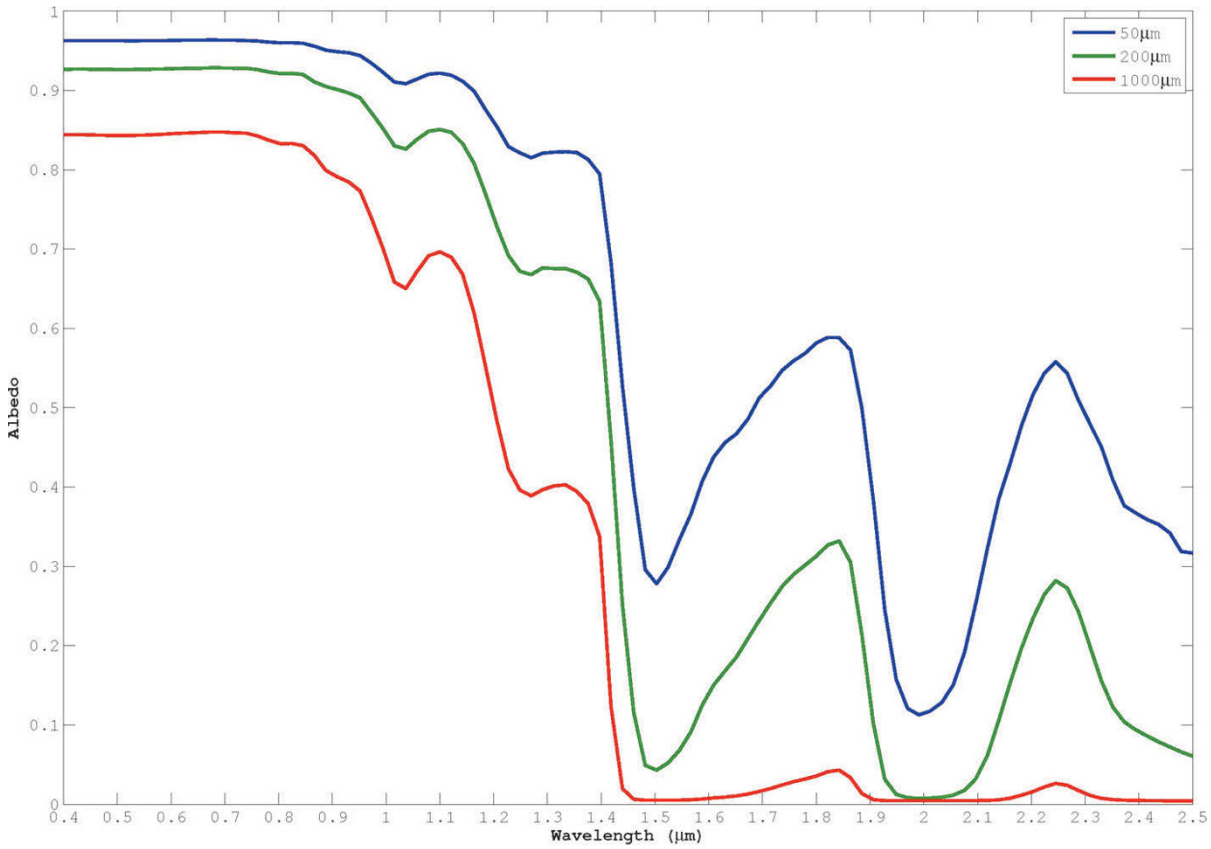

Figure 3.6. RT-based model of spectral albedo for a layer of an optically thick mixture of pure snow and carbon soot as a function of wavelength and snow grain size (50, 200, and 1,000 μm). Soot particle concentration is assumed to be 3 ppmw. The optical properties of the two constituents have been independently computed using Mie theory. Figure can also be viewed as Online Supplement 3.6.

theory is used to compute single-particle optical properties. As expected, the angle of incidence of the incoming radiation illuminating the snowpack has a large effect on albedo. As shown in Fig. 3.5, albedo increases with increasing solar zenith angle. Wiscombe and Warren (1980) explained this phenomenon by postulating that, because of the high inclination with respect to the zenith, photons entering the medium travel close to the upper surface of the snowpack and therefore scattering events give light particles a higher probability of exiting the snowpack surface.

In the third set of simulations, a RT model was employed to compute the spectral albedo of a layer of an optically thick mixture of pure snow and carbon soot as a function of grain size (50, 200, and 1,000 μm; see Fig. 3.6). The optical properties of the two constituents have been independently computed using Mie theory. The optical properties of carbon soot were computed (assuming the soot particles are modeled as spheres) by setting the soot radius equal to 0.1 μm and particle density equivalent to 0.3 ppmw (parts per million weight). The soot complex index of refraction is assumed to be constant across the spectral range of interest and equal to $1.95 + 0.79i$. Fig. 3.6 shows the resulting spectral albedo as a function of wavelength along with the radius of the snow particles. Simulations show that a small amount of carbon soot is sufficient to lower albedo in the visible region of the spectrum where ice has the lowest absorption (highly scattering media with single-scattering albedo very close to one). As expected, albedo reduction is more marked for larger snow particles. Relatively high scattering between 0.4 μm and 0.7 μm increases the probability that photons are more likely to experience multiple scattering, therefore increasing the probability of encountering a carbon particle and being absorbed. As discussed above, increasing snow particle grain size increases average free mean path, further increasing the probability of encountering a carbon particle and being absorbed.

Table 3.1. Input optical parameters employed for MADOC BRF simulations of intimate and areal mixtures of ice and soil.

Parameters	*Ice*	*Soil*
Wavelength (μm)	0.63	0.63
Particle diameter (μm)	30	10
Variance	0.2	0.1
Distribution	Log normal	Modified gamma
Index of refraction (real)	1.31	1.55
Index of refraction (imag)	0	0.001
Max radius	35	N/A
Min radius	25	N/A
Single-scattering albedo	1	0.85413
Max scattering coefficients	641	641
Type of simulation	Intimate mixture	Intimate mixture

In the NIR region (above 0.9 μm) the influence of carbon particles on albedo is limited, as its reduction is dominated by the stronger absorption of ice. This simulation shows that carbon soot and generally other impurities (e.g., dust; Wiscombe and Warren 1980) may have a large impact on the overall energy budget of glaciers.

The fourth set of simulations shows an example of a BRF for an optically thick mixture of soil and ice as a function of the percentage volume of the two pure components. The mixture BRF was computed at a specified wavelength in the visible region of the spectrum (0.63 μm). Input parameters, including the complex index of refraction, grain size, and grain size distribution for both soil and snow are reported in Table 3.1 (Warren 1984, Mishchenko et al. 1999). A total of 641 coefficients of the Legendre expansion were used to properly describe the phase function. Fig. 3.7 demonstrates the reflectance variability associated with intimate mixtures of ice and sediment/soil. Clearly, the magnitude of reflectance decreases as the percentage of sediment/soil increases. The anisotropic nature of reflectance is also noteworthy, as pure ice exhibits a highly variable pattern that is directionally dependent. The anisotropic pattern changes with increasing sediment, such that azimuthal reflectance variations become more spatially homogeneous. The forward-scattering component also decreases in extent and magnitude, while the backscatter component decreases in extent, and exhibits an increase in magnitude associated with increasing debris.

In the fifth set of simulations, the reflectance patterns of typical glacier lake water were computed as a function of particle and phytoplankton concentration, wind speed, and sensor geometry. Fig. 3.8 depicts spectral curves from 390 to 710 nm. Simulations were implemented using the analytical fit of HYDROLIGHT for Case 2 (turbid) waters (Albert and Mobley 2003). Clearly, increasing the suspended matter content tends to decrease reflectance variability (flatten spectral curves) and increase the magnitude of reflectance from the lake

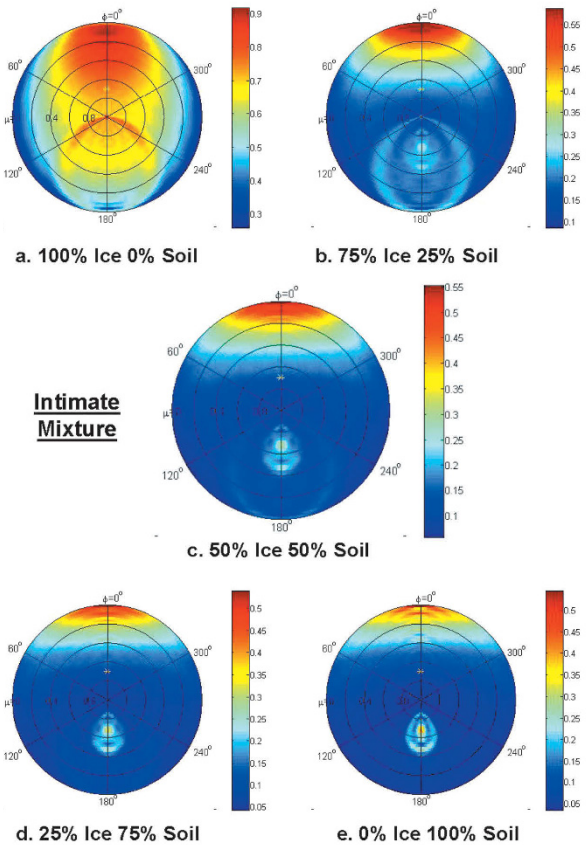

Figure 3.7. BRF simulations for intimate mixtures (in volume percentage) of ice and sediment/soil. The overall magnitude (i.e., albedo) decreases as the percentage of soil increases. BRF patterns are also a function of the mixture percentage. This set of simulations shows that BRF patterns can be potentially used to discriminate between various surface materials and conditions in glacier environments. Figure can also be viewed as Online Supplement 3.7.

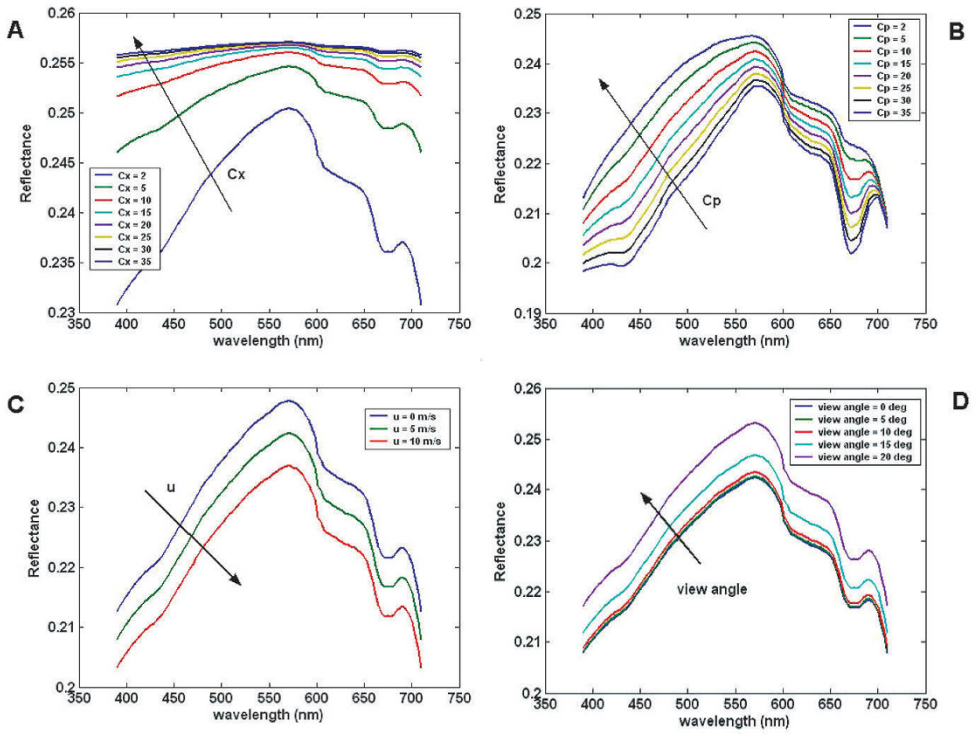

Figure 3.8. Simulated spectral reflectance curves from 390 nm to 710 nm as a function of suspended particles and phytoplankton concentrations, wind speed, and Sun angle. Simulations are based on an analytical fit of the HYDROLIGHT radiative transfer model adapted to simulate Case 2 water. (A) Effect of suspended matter on deep-lake water reflectance. As concentration increases, spectral variability decreases, although the magnitude of reflectance increases across the wavelength range. (B) Effect of phytoplankton, causing increased reflectance with a peak in the green region of the spectrum. (C) Effect of wind speed (u) on spectral reflectance. A decrease in wind speed results in higher reflectance. (D) Effect of solar zenith angle on reflectance. The range of angles causes a small change in reflectance but no significant change in absorption. Figure can also be viewed as Online Supplement 3.8.

water surface. In fact, as the particle concentration increases, scattering dominates over absorption. In addition, measurements over Lake Constance water (Gege 1998, Heege 2000) showed that scattering (and backscattering) is fairly insensitive to wavelength. In most cases, glacier lake turbidity is so high that large optical depths effectively preclude transmittance of light that has reflected off the lake bottom, except in uncommon cases of extremely shallow lakes and areas fringing the edges of deep lakes. The more usual bathymetry of glacier lakes causes very narrow edge zones where the bottom is sensed, so to a good approximation one can completely ignore bottom reflectance and assume a condition of infinite optical thickness. However, by modifying bottom boundary conditions (i.e., assuming that the bottom of the lake is reflecting), RT code for water can be employed to compute the spectral reflectance of shallow lakes. Importantly, such simulations require guestimating the spectral reflectance properties of the lake bottom.

3.6 CONCLUSIONS

Radiative transfer theory is a powerful tool that can be employed to quantify the amount of radiation reflected by glacier surfaces and glacier lake water. The equations of radiative transfer, which describe the balance of photons that are being absorbed and scattered in their interaction with the host medium, are mathematically complex. Nevertheless, over the past few decades, advancements in numerical modeling of RTEs have provided the scientific community with RT software that permits the computation of physical quantities of interest in remote sensing (e.g., BRF and spectral albedo) both efficiently and accurately. Such RTE-based radiance calculations, however, are only meaningful if knowledge of the medium's optical properties is available. Such RTEs require the input of explicit models for single-scattering albedo and scattering phase function, which in turn depend upon the use of absorption and scattering coefficients (as well as

efficiencies), the asymmetry parameter (or Legendre coefficients describing series expansion of the phase function), particle concentrations, wavelength of interest, as well as size and shape of the single-type particles/mixture of many-type particles describing the medium. Mie theory is the most popular way to determine such properties.

Based on the assumption that a single particle is spherical, Mie-based code has been designed to compute the aforementioned parameters as a function of the complex index of refraction and particle size. The spherical particle assumption has been shown not to be limiting for snow and ice mixtures, but does not accurately model soil/sediment optical properties. More advanced techniques based on the T-matrix and ray-tracing methods have been designed to model the optical properties for particles of irregular shape. Nevertheless, they tend to be computationally expensive.

The optical properties of glacier lake water have been modeled by experimentally determining the scattering and absorption coefficient of the various components comprising the host medium (pure water, phytoplankton, particle concentration, CDOM). Models for a scattering phase function that is suitable to describe the in-scattering of Case 2 waters has also been proposed.

The RT simulation examples have demonstrated that modeling can be effectively employed as an investigative tool to assess the information content in satellite imagery. Furthermore they show how typical glacier surface conditions and glacial lakes optically respond as a function of their morphological and mineralogical composition. Consequently, the coupling of RT modeling and multispectral digital image analysis can be used to assess important biophysical parameters of glacier environments, such that the assimilation of sensor data can produce spatiotemporal quantitative information regarding the observed medium including ice grain size, percentage of carbon soot in snow, concentration of glacier flour in lakes, pixel debris cover percentages. Such attempts or algorithms are usually called "physically based inversion algorithms", and they are essentially models based on first principles which are employed to describe the functional inverse relationship between a sensor-collected signal and the properties of the observed surface/medium (Furfaro 2004, Furfaro et al. 2007, Picca et al. 2008b). It is important to note, however, that such RT and coupling issues can be difficult problems to solve. Indeed, it is well known that inverse problems are ill posed in that they do not depend continuously on the data. Recent mathematical advancements in the field of statistics applied to machine learning (e.g., neural networks, Gaussian processes, regularized sliced inverse regression), however, have made model inversion more manageable. Examples of such approaches can be found in the literature for a variety of applications in Earth and planetary science (e.g., Furfaro et al. 2007, Morris et al. 2008, Bernard-Michel et al. 2009). The latter reinforce the significance of RT modeling for studying and understanding the Earth's cryosphere.

3.7 REFERENCES

Albert, A., and Mobley, C.D. (2003) An analytical model for subsurface irradiance and remote sensing reflectance in deep and shallow case-2 waters. *Optics Express*, **11**(22), 2873–2890.

Aoki, T., Aoki, T., Fukabori, M., Hachikubo, A., Tachibana, Y., and Nishio, F. (2000) Effects of snow physical parameters on spectral albedo and bidirectional reflectance of snow surface. *Journal of Geophysical Research*, **105**, 10219–10236.

Bernard-Michel, C., Douté, S., Fauvel, M., Gardes, L., and Girard, S. (2009) Retrieval of Mars surface physical properties from OMEGA hyperspectral images using regularized sliced inverse regression. *Journal of Geophysical Research (Planets)*, **114**, 6005.

Bishop, M.P., Barry, R.G., Bush, A.B.G., Copland, L., Dwyer, J.L., Fountain, A.G., Haeberli, W., Hall, D.K., Kääb, A., Kargel, J.S. et al. (2004) Global land-ice measurements from space (GLIMS): Remote sensing and GIS investigations of the Earth's cryosphere. *Geocarto International*, **19**(2), 57–84.

Bohren, C.F. (1983) Colors of snow, frozen waterfall and icebergs. *J. Opt. Soc. Am.*, **73**, 1646–1652.

Bohren, C.F. and Barkstrom, B.R. (1974) Theory of the optical properties of snow. *Journal of Geophysical Research*, **79**, 4527-4535.

Bush, A.B.G. (2000) A positive feedback mechanism for Himalayan glaciation. *Quaternary International*, **65**(6), 3–13.

Chandrasekhar, S. (1960) *Radiative Transfer*, Dover, New York.

Davis, A.B., and Knyazikhin, Y. (2005) A primer in 3D radiative transfer. *3D Radiative Transfer in Cloudy Atmospheres*, Vol. 2, Springer-Verlag, Berlin, pp. 153–242.

de Hann, J.F., Bosma, P.B., and Hovenier, J.W. (1987) The adding method for multiple scattering calculations of polarized light. *Astron. Astrophys.*, **183**, 371–391.

Dozier, J., Davis, R.E., and Perla, R. (1987) On the objective analysis of snow microstructure. In: B. Salm and H. Gubler (Eds.), *Avalanche Formation, Movement*

and Effects (IAHS Pub. No. 62), International Association of Hydrological Sciences, Wallingford, U.K., pp. 49–59.

Fournier, G.R., and Fourand, J.L. (1994) Analytical phase function for ocean water. In: J.S. Jaffe (Ed.), *Ocean Optics XII* (Proc. SPIE 2258), Society of Photo-Optical Instrumentation Engineers, Bellingham, WA, pp. 194–201.

Furfaro, R. (2004) Radiative transport in plant canopies: Forward and inverse problem for UAV applications. Ph.D. Dissertation, University of Arizona.

Furfaro, R., Ganapol, B.D., Johnson, L.F., and Herwitz, S.R. (2007) Coffee ripeness monitoring with airborne imagery: Neural network algorithm for field ripeness evaluation using reduced a priori information. *Applied Engineering in Agriculture*, **23**, 379–387.

Furfaro, R., Previti, A., Picca, P., Mostacci, D., Ganapol, B.D. (2014) Multi-layer Analytic Discrete Ordinate Code (MADOC): An accurate and efficient radiative transfer platform to compute the bidirectional reflectance factor and spectral albedo of highly inhomogeneous planetary surfaces. *Journal of Quantitative Spectroscopy and Radiative Transfer* (in preparation).

Ganapol, B.D., and Furfaro, R. (2008) *The Art of Analytical Benchmarking* (Lecture Notes in Computational Science and Engineering, Vol. 62), Springer-Verlag, New York, pp. 105–134.

Gege, P. (1998) Characterization of the phytoplankton in Lake Constance for classification by remote sensing. *Arch. Hydrobiolog. Adv. Limnology*, **53**, 179–193.

Haeberli, W., and Beniston, M. (1998) Climate change and its impacts on glaciers and permafrost in the Alps. *Ambio*, **27**(4), 258–265.

Hansen, J.E. and Travis, L.D. (1974) Light scattering in planetary atmospheres. *Space Sci. Rev.*, **16**, 527–610.

Hapke, B.W. (1981) Bidirectional reflectance spectroscopy, 1: Theory, *Journal of Geophysical Research*, **86**, 3039–3054.

Hapke, B.W. (1986) Bidirectional reflectance spectroscopy, 4: The extinction coefficient and the opposition effect. *Icarus*, **67**, 264–280.

Hapke, B.W. (1993) *Theory of Reflectance and Emittance Spectroscopy*, Cambridge University Press, New York.

Hapke, B. (2002) Bidirectional reflectance spectroscopy, 5: The coherent backscatter opposition effect and anisotropic scattering. *Icarus*, **157**, 523–534.

Hapke, B. (2008) Bidirectional reflectance spectroscopy, 6: Effects of porosity. *Icarus*, **195**, 918–926.

Heege, T. (2000) Flugzeuggestuzte Fernerkundung von Wasserinhaltsstoffen im Bodensee, PhD thesis, Remote Sensing Technology Institute, German Aerospace Center (DLR).

Helfenstein, P., Veverka, J., and Thomas, P. (1988) Uranus satellites: Hapke parameters from Voyager disk-integrated photometry. *Icarus*, **74**, 231–239.

Jin, Z., Charlock, T.P., Rutledge, K., Stamnes, K., and Wang, Y. (2006) An analytical solution of radiative transfer in the coupled atmosphere–ocean system with rough surface. *Applied Optics*, **45**, 7443–7455.

Kargel, J.S., Abrams, M.J., Bishop, M.P., Bush, A., Hamilton, G., Jiskoot, H., Kääb, A., Kieffer, H.H., Lee, E.M., Paul, F. et al. (2005) Multispectral imaging contributions to global land ice measurements from space. *Remote Sensing of the Environment*, **99**, 187–219.

Kotlyakov, V.M., Serebrjanny, L.R., and Solomina, O.N. (1991) Climate change and glacier fluctuations during the last 1,000 years in the southern mountains of the USSR. *Mountain Research and Development*, **11**, 1–12.

Lewis, E.E., and Miller, W.F. (1984) *Computational Methods of Neutron Transport*, Wiley-Interscience, New York.

Macke, A., Mueller, J., and Raschke, E. (1996) Single scattering properties of atmospheric ice crystals. *Journal of Atmospheric Sciences*, **53**(19), 2813–2825

Mackowski, D.W., and Mishchenko, M.I. (1996) Calculation of the T matrix and the scattering matrix for ensembles of spheres. *J. Opt. Soc. Am. A*, **13**, 2266–2278.

Mackowski, D.W., and Mishchenko, M.I. (2011) A multiple sphere T-matrix Fortran code for use on parallel computer clusters. *Journal of Quantitative Spectroscopy and Radiative Transfer*, **112**(13), 2182–2192.

Maisch, M. (2000) The longterm signal of climate change in the Swiss Alps: Glacier retreat since the end of the Little Ice Age and future ice decay scenarios. *Geografia Fisica e Dinamica Quaternaria*, **23**(2), 139–151.

Marston, P.L., Langley, D.S., and Kingsbury, D.L. (1982) Light scattering by bubbles in liquids: Mie theory, physical optical approximations and experiments. *Applied Science Research*, **38**, 373–383.

Matzler, C. (2004) Matlab codes for Mie Scattering and absorption. Available at *http://diogenes.iwt.unibremen.de/vt/laser/wriedt/Mie_Type_Codes/body_mie_type_codes.html*

Meier, M.F., and Wahr, J.M. (2002) Sea level is rising: Do we know why? *Proceedings of the National Academy of Science*, **99**(10), 6524–6526.

Mishchenko, M.M., Dlugach, J.M., Yanovitskij, E.G., and Zakharova, E.T. (1999) Bidirectional reflectance of flat, optically thick particulate layers: An efficient radiative transfer solution and applications to snow and soil surfaces. *Journal of Quantitative Spectroscopy and Radiative Transfer*, **63**, 409–432.

Mobley, C.D. (1994) *Light and Water Radiative Transfer in Natural Waters*. Academic Press, New York.

Mobley, C.D., Sundman, L.K., and Boss, E. (2002) Phase function effects on oceanic light fields. *Applied Optics*, **41**, 1035–1050.

Morris, R.D., Kottas, A., Furfaro, R., Taddy, M., and Ganapol, B. (2008) A statistical framework for the sensitivity analysis of radiative transfer models used in remote sensed data product generation. *IEEE Trans. Geosci. Remote Sens.*, **46**(12), 4062–4074.

Mugnai, A., and Wiscombe, W.J. (1980) Scattering of radiation by moderately nonspherical particles. *Journal of Atmospheric Science*, **37**, 1291–1307

Mullen, P.C., and Warren, S.G. (1988) Theory of the optical properties of lake ice. *Journal of Geophysical Research*, **93**, 8403–8414.

Painter, T.H., Dozier, J., Roberts, D.A., Davis, R.E., and Green, R.O. (2003) Retrieval of subpixel snow-covered area and grain size from imaging spectrometer data. *Remote Sensing of Environment*, **85**(1), 64–77.

Petzold, T.J. (1972) *Volume Scattering Functions for Selected Ocean Waters* (SIO Ref. 71–78), Scripps Institute of Oceanography, San Diego, CA.

Piatek, J., Hapke, B., Nelson, R., Smythe, W., and Hale, A. (2004) Scattering properties of planetary regolith analogs. *Icarus*, **171**, 531–545.

Picca, P. (2009) Applications of the Boltzmann equation to the neutronics of nuclear reactors and to radiative transfer, PhD thesis, Politecnico di Torino.

Picca, P., Furfaro, R., and Ganapol, B.D. (2007) Extrapolated iterative solution for the transport equation in inhomogeneous media. *Transactions of American Nuclear Society*, **97**, 627–629.

Picca, P., Furfaro, R., and Ganapol, B.D. (2008a) Optimization of the extrapolated iterative method for the multislab transport problem. Paper presented at *PHYSOR 2008, Interlaken, September 14–19, 2008*.

Picca, P., Furfaro, R., Kargel, J., and Ganapol, B. (2008b) Forward and inverse models for photon transport in soil–ice mixtures and their application to the problem of retrieving optical properties of planetary surfaces. *Space Exploration Technologies* (Proc. SPIE, 6960), Society of Photo-Optical Instrumentation Engineers, Bellingham, WA (11 pp.).

Pope, R.M., and Fry, E.S. (1997) Absorption spectrum (380–700 nm) of pure water, II: Integrating cavity measurements. *Appl. Opt.*, **36**, 8710–8723.

Previti, A. (2010) Semi-analytic radiative transfer model for remote sensing of planetary surfaces, Tesi Di Laurea Specialistica, Alma Mater Studiorum, Università di Bologna.

Previti, A., Furfaro, R., Picca, P., Ganapol, B.D., and Mostacci, D. (2011) Solving radiative transfer problems in highly heterogeneous media via domain decomposition and convergence acceleration techniques. *Applied Radiation and Isotopes*, **69**(8), 1146–1150.

Prieur, L., and Sathyendranath, S. (1981) An optical classification of coastal and oceanic waters based on the specific absorption of phytoplankton pigments, dissolved organic matter, and other particulate materials. *Limnol. Oceanogr.*, **26**, 671–689.

Seltzer, G.O. (1993) Late-Quaternary glaciation as a proxy for climate change in the central Andes. *Mountain Research and Development*, **13**, 129–138.

Shroder, J.F., Jr., and Bishop, M.P. (2000) Unroofing of the Nanga Parbat Himalaya. In: M.A. Khan, P.J. Treloar, M.P. Searle, and M.Q. Jan (Eds.), *Tectonics of the Nanga Parbat Syntaxis and the Western Himalaya* (Special Publication No. 170), Geological Society, London, pp. 163–179.

Siewert, C.E. (1978) The FN method for solving radiative-transfer problems in plane geometry. *Astrophysics and Space Science*, **58**, 131–137.

Siewert, C.E. (2000) A concise and accurate solution to Chandrasekhar's basic problem in radiative transfer. *Journal of Quantitative Spectroscopy and Radiative Transfer*, **64**, 109–130.

Stamnes, K., Tsay, S.-C., Wiscombe, W.J., and Jayaweera, K. (1988) Numerically stable algorithm for discrete-ordinate-method radiative transfer in multiple scattering and emitting layered media. *Applied Optics*, **27**, 2502–2509.

Warell, J., Sprague, A., Kozlowski, R., and Helbert, J. (2009) Surface composition and chemistry of Mercury: Hapke modeling of MESSENGER/MASCS reflectance spectra. *Lunar Planet. Sci.*, **40**, 1902.

Warren, S.G. (1984) Optical constants of ice from the ultraviolet to the microwave. *Appl. Opt.*, **23**(8/15).

Warren, S.G., and Brandt, R.E. (2008) Optical constants of ice from the ultraviolet to the microwave: A revised compilation. *Journal of Geophysical Research*, **113**, D14220.

Waterman, P.C. (1971) Symmetry, unitarity, and geometry in electromagnetic scattering. *Phys. Rev. D*, **3**, 825.

Wiscombe, W.J. (1980) Improved Mie scattering algorithms. *Applied Optics*, **19**(9), 1505–1509.

Wiscombe, W.J. (1996) *Mie Scattering Calculations: Advances in Technique and Fast, Vector-Speed Computer Codes* (NCAR/TN-140 + STR), National Center for Atmospheric Research, Boulder, CO.

Wiscombe, W. and Warren, S. (1980) A model for the spectral albedo of snow, I: Pure snow. *Journal of Atmospheric Science*, **37**, 2712–2733.

Yang, P., and Liou, K.N. (1998) Single-scattering properties of complex ice crystals in terrestrial atmosphere. *Contrib. Atmos. Phys.*, **71**, 223–248.